Table 1 Chemical state summary

	$(H \rightarrow H^+ + e^-)$ Stagnation region	Cone flank
Uranus (warm, nominal)	frozen	frozen
Uranus (cool)	equilibrium	equilibrium
Saturn (warm)	frozen	frozen
Saturn (nominal)	nonequilibrium	equilibrium
Saturn (cool)	~ equilibrium	equilibrium
Jupiter	equilibrium	equilibrium

For a binary mixture of molecular hydrogen and helium, Eq. (11) may be expressed as

$$T_s = \varepsilon(1-\varepsilon)(X_2 M_2 + X_1 M_1)_s U^2 \cos^2\theta_s / R \tag{13}$$

and Eq. (7) becomes

$$\frac{\tau_{\text{ion}}}{\tau_f} = \frac{10^{-15}(X_2 M_2 + X_1 M_1)_s U \cos\theta \exp(1.151 \times 10^5 / T_s)}{\rho_\infty \delta X_{H_{2_s}} \left(2\sum X_i \frac{\hat{c}_{p_i}}{R} - 1\right)_s^2} \tag{14}$$

For H_2 and He, $\hat{c}_{p_i}/R$ is 4.5 and 2.5, respectively, and, as noted, X_1 and X_2 are 0.208 and 0.792. For a standoff distance of 1 cm at the stagnation point, the locus of $\tau_{\text{ion}}/\tau_f = 0.1$ is shown as a function of flight conditions ρ_∞ and U in Fig. 2 by the double dashed line. Equilibrium exists above the line for that mixture.

For 100% H_2, we use the result of Fig. 9 of Ref. 1 and note that

$$l_{\text{ion}} = \varepsilon U \tau_{\text{ion}} \tag{15}$$

and from Eq. (4) we obtain

$$\frac{\tau_{\text{ion}}}{\tau_f} = \frac{\varepsilon U l_{\text{ion}} \cos\theta}{\varepsilon U x} = \frac{(\rho_\infty l_{\text{ion}})\cos\theta}{\rho_\infty x} = \left(\frac{p_\infty l_{\text{ion}} M_\infty}{R T_\infty}\right)\frac{\cos\theta}{\rho_\infty x} \tag{16}$$

Although the data are given as $p_\infty l_{\text{ion}}$ as a function of U, the important parameter is $\rho_\infty l_{\text{ion}}$, which is obtained from Eq. (16) for $T_\infty = 300°$K. Accordingly, the loci of $\tau_{\text{ion}}/\tau_f = 0.1$ and 10.0 are shown in Fig. 2 by the double solid curve and the single dashed curve, respectively, as a function of the flight conditions ρ_∞ and U, again for a standoff distance of 1 cm. Chemical equilibrium exists above the upper curve, nonequilibrium between the two, and, essentially, frozen flow below the lower curve for pure H_2.

Some representative entry trajectories for Saturn, Uranus, and Jupiter are also plotted on the figure. Peak heating is shown by the lettered solid symbol in each case. For Jupiter, the atmospheric composition is approximately 85% H_2, 15% He, and the equilibrium line probably lies somewhat below the symbol D; that is, for the highly energetic Jupiter entry, the ionization relaxation would be complete before the point of maximum heating. At the other extreme, for the nominal Uranus atmosphere (95% H_2, 4% He),[5] curve C indicates that the reaction (1) would be frozen.

A summary of these estimates for entry into the various model atmospheres of the outer planets is shown in Table 1 for both the stagnation region and for the flank of a 60° half-angle cone having a 1-m ray. Interestingly, finite rate chemistry seems to play a role only for entry into the Saturn nominal atmosphere (79% H_2, 20% He) at a fairly steep entry angle (40°). For shallow entry (15°) into that atmosphere, the reaction (1) would probably be frozen. Thus, except for the steep entry into the Saturn nominal atmosphere, the computation of all entry probe gascaps for the outer planets can probably be considered on either a frozen or a chemical equilibrium basis and avoid the complications of finite rate chemistry.

References

[1] Leibowitz, L. P., "Measurements of the Structure of an Ionizing Shock Wave in a Hydrogen-Helium Mixture," *The Physics of Fluids*, Vol. 16, No. 1, Jan. 1973, pp. 59–68.

[2] Page, W. A., private communication, 1973, NASA.

[3] Howe, J. T., Viegas, J. R., and Sheaffer, Y. S., "Study of the Nonequilibrium Flow Field Behind Normal Shock Waves in Carbon Dioxide," TN D-1885, June 1963, NASA.

[4] Howe, J. T. and Sheaffer, Y. S., "Chemical Relaxation Behind Strong Normal Shock Waves in Carbon Dioxide Including Interdependent Dissociation and Ionization Processes," TN D-2131, Feb. 1964, NASA.

[5] *The Planets Uranus, Neptune, and Pluto (1971)*, NASA SP-8103, Nov. 1972.

Role of Plasma Boundary Conditions in the Comparison of Electron Plasma Temperatures

A. SINGER* AND J. M. MINKOWSKI†

The Johns Hopkins University, Baltimore, Md., and Harry Diamond Laboratories, Washington, D.C.

Introduction

THE first two attempts[1,2] to determine the electron temperature of shock-heated plasma by microwave techniques yielded results that cannot be meaningfully compared with the values predicted by shock-wave theory, either because insufficient plasma parameters were measured[1] or because there is considerable doubt as to whether the plasma was in thermal equilibrium.[2] Avoiding these pitfalls, Aro and Walsh[3] obtained values for electron temperature of shock-heated argon (initially at 4 torr and room temperature) over a very large electron density range, 10^{16}–10^{22} m^{-3}, corresponding to shock levels of Mach 6.8–10.5, by means of a set of microwave horns and an associated superheterodyne receiver centered at 9.05 GHz. However, a prominent feature of the Aro-Walsh experiment was that the results significantly exceeded the theoretically predicted values in three Mach regions: below Mach 7.4, between Mach 8.0 and 8.8, and above Mach 9.7, corresponding to electron densities, n_e, below 4×10^{18}, between 5×10^{19} and 6×10^{20}, and above 4×10^{21} m^{-3}. This was particularly puzzling because no plausible physical mechanism could be found to account for this anomaly. In order to check whether these results were genuine, Aro and Walsh performed another experiment in which they viewed the same plasma in a waveguide probe.[4] Since the waveguide probe results were in much closer agreement with theory and almost consistently lower than the theoretical values, they concluded that the anomalies were due to a plasma boundary layer associated with the aerial geometry of the microwave-horn experiment.

It has been recently shown,[5] however, that in the upper Mach region (above 9.7) the anomaly was only apparent and was in

Received December 13, 1973. The stimulating discussions with G. Bekefi of MIT and M. Apstein of the Harry Diamond Labs. were very helpful and are gratefully acknowledged. We would also like to thank W. E. Phillips of the National Bureau of Standards for reviewing the manuscript.

Index categories: Plasma Dynamics and MHD; Shock Waves and Detonations.

* Research Associates, Department of Electrical Engineering; also Research Engineer, Harry Diamond Laboratories.

† Associate Professor, Department of Electrical Engineering.

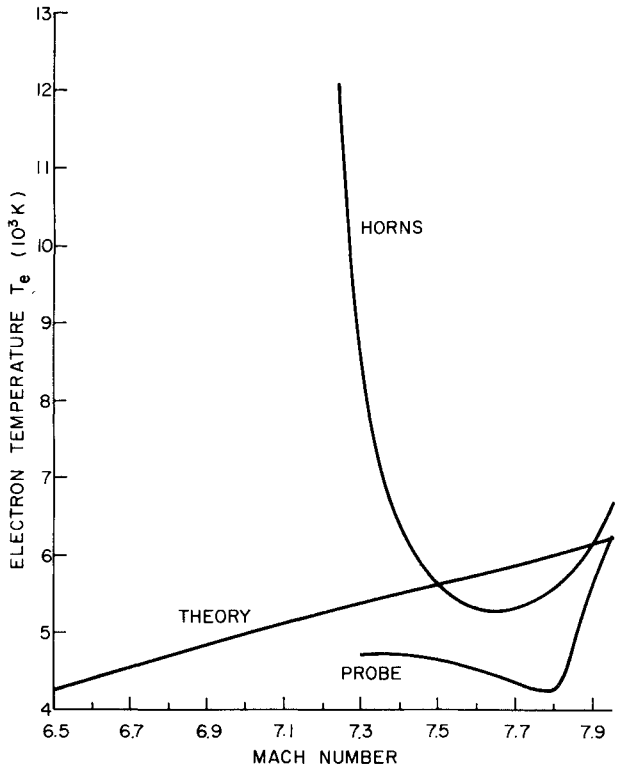

Fig. 1 Electron temperature of shock-heated argon initially at 4 torr and room temperature, at relatively low shock levels, as determined by means of microwave horns,[3] a waveguide probe,[4] and shock-wave theory.[3]

fact due to an incorrect model for relating the measured plasma parameters to the electron temperature. It also has been shown[6] that in the middle and upper Mach regions, the waveguide probe results may not completely represent the electron plasma temperatures. It is the purpose of this Note to show that in the lower Mach region (below 7.4) the results obtained by the two Aro-Walsh experiments cannot be compared directly on a one-to-one basis, but allowance must first be made for a shift in the general form of the waveguide probe results towards lower densities to account for the radically different plasma boundary conditions.

Electron Temperature

In both experiments[3,4] Aro and Walsh determined the electron plasma temperature, t_e, from the following equation[7]

$$t_e = \frac{t_r}{1-R-T} = \frac{t_r}{(1-R)(1-e^{-\alpha L})} \tag{1}$$

where t_r is the measured radiation temperature; R and T are the power reflection and transmission coefficients, respectively; α is the absorption per unit length; and L is the effective plasma thickness. R and T were measured directly; t_r was determined by dividing the measured radiation power by kB, where k is Boltzmann's constant and B is the i.f. bandwidth of the superheterodyne receiver used in the measurement.

Figure 1 compares the electron plasma temperatures obtained by means of the two techniques in the low density region, i.e., below $n_e = 4 \times 10^{18}$ m^{-3} or Mach 7.4. The reason the microwave-horn results are not shown below Mach 7.2 ($n_e = 1.5 \times 10^{18}$ m^{-3}), even though the measurements were made down to Mach 6.8 ($n_e = 1.7 \times 10^{17}$ m^{-3}), is that Eq. (1) diverges when the Aro-Walsh measured plasma parameters for this region are substituted into it. On the other hand, the reason the waveguide probe results are not shown in Fig. 1 below Mach 7.3 ($n_e = 2.5 \times 10^{18}$ m^{-3}), even though here the measurements were made down to Mach 6.5 ($n_e = 1.5 \times 10^{16}$ m^{-3}), stems from a basic shortcoming in the technique itself: since the transmission coefficient, T, cannot be readily measured by means of the waveguide probe, the technique is limited to electron densities at which the magnitude of T may be assumed to be zero. Using an earlier experiment[3] on the same plasma as a guide, Aro and Walsh were able to justify such an assumption above Mach 7.3 ($n_e = 2.5 \times 10^{18}$ m^{-3}), but not below that level.

Effect of Boundary Conditions

In the microwave-horn experiment, the measuring system is looking at a 2-in.-diam cylindrical plasma slug, approximately 1–2.5 ft high (depending on the shock level), with the polarization of the probing signal perpendicular to the axis of the cylinder. Thus, here the absorption per unit length, α_H, is very close to that of an infinitely large plasma, and may be approximated by[8]

$$\alpha_H = (2)^{1/2}\frac{\omega}{c}\left\{-\left(1-\frac{(\omega_p/\omega)^2}{1+(\nu/\omega)^2}\right)+\left[\left(1-\frac{(\omega_p/\omega)^2}{1+(\nu/\omega)^2}\right)^2+\left(\frac{\nu/\omega(\omega_p/\omega)^2}{1+(\nu/\omega)^2}\right)^2\right]^{1/2}\right\}^{1/2} \tag{2}$$

where ω is the radian frequency under consideration; c is the speed of light; ν is the electron collision frequency; and ω_p is the electron plasma frequency given by $\omega_p{}^2 = n_e e^2/m\varepsilon_o$, with n_e the plasma electron number density, e the electronic charge, m the electronic mass, and ε_o the permittivity of free space. In many cases, the electron collision frequency may be approximated by[9]

$$\nu = 3.62 \times 10^{-6}\frac{n_i}{t_e^{3/2}}\ln\left(1.23 \times 10^7 \frac{t_e^{3/2}}{n_e^{1/2}}\right)+2.6 \times 10^4 \sigma^2 n_n t_e^{1/2} \tag{3}$$

where n_i, n_e, and n_n are the ion, electron, and neutral densities (m^{-3}), respectively; t_e is the electron plasma temperature in °K; and σ is the collision diameter (m) for electron-neutral collisions.

In the waveguide probe experiment, on the other hand, we have a plasma loaded X-band rectangular waveguide and a 9.05-GHz $TE_{1,0}$ wave as a probing signal. Therefore, here the absorption per unit length, α_W, may be approximated by[10]

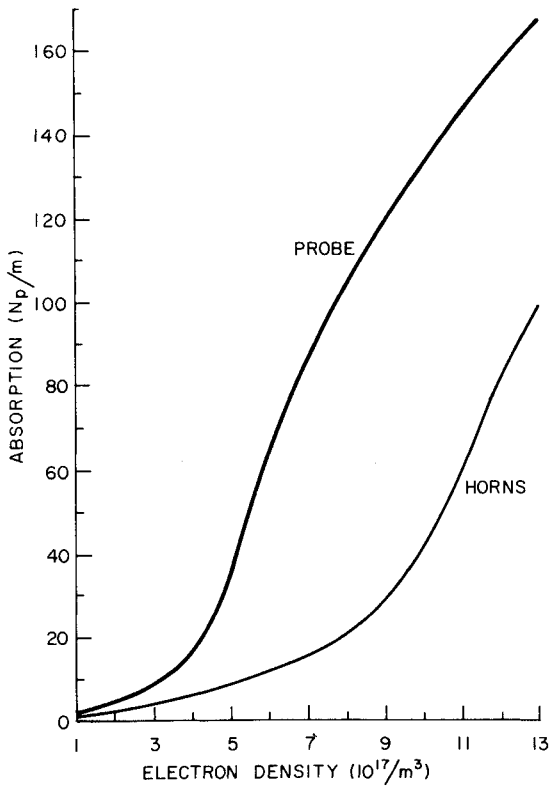

Fig. 2 Plasma absorption per unit length vs electron density, computed for the two Aro-Walsh experiments.

$$\alpha_W = (2)^{1/2}\frac{\omega}{c}\left\{-\left(1-\frac{\omega_c^2}{\omega^2}-\frac{(\omega_p/\omega)^2}{1+(\nu/\omega)^2}\right)+\left[\left(1-\frac{\omega_c^2}{\omega^2}-\frac{(\omega_p/\omega)^2}{1+(\nu/\omega)^2}\right)^2+\left(\frac{\nu/\omega(\omega_p/\omega)^2}{1+(\nu/\omega)^2}\right)^2\right]^{1/2}\right\}^{1/2} \quad (4)$$

where ω_c is the waveguide mode cutoff frequency in the absence of plasma, and the rest of the parameters have been defined earlier.

The curves comparing the salient features of the plasma absorption per unit length (α_H and α_W) for the two Aro-Walsh experiments are shown in Fig. 2. It is seen that, as far as the measuring system is concerned, the major effect of the waveguide boundary condition is an apparent increase in the electron plasma density. In other words, the measuring system essentially cannot tell whether a waveguide boundary has been imposed on the plasma or whether the plasma density has in fact increased. Thus, it would not be meaningful to compare the two experimental curves for electron temperature (of Fig. 1) on a one-to-one basis but allowance must first be made for a shift in the general features of the waveguide probe results toward lower actual plasma densities or shock levels.

For the 9.05-GHz center frequency considered here, the critical plasma density is about 10^{18} m^{-3}, yielding a "knee" in the absorption curve for the microwave-horn experiment at about Mach 7.1 (Fig. 2); whereas in the waveguide probe experiment, the knee in the absorption curve is at about Mach 6.95, corresponding to a virtual critical density of about 3.5×10^{17} m^{-3} (Fig. 2), or about a factor of three lower. In the microwave-horn experiment the electron plasma temperatures exceed the theoretical values between Mach 6.8 and 7.4, corresponding to plasma densities between about 1.5×10^{17} and 4×10^{18} m^{-3}, or between about 0.15 and 4 times the critical density. Thus, if the results of the waveguide probe experiment were to exhibit the same type of anomalous form at relatively low densities, we would expect it to occur between about 0.15 and 4 times the *virtual* critical density (for this case 3.5×10^{17} m^{-3}), corresponding to shock levels between Mach 6.6 and 7.2. However, as discussed earlier, the electron temperature could not be computed below Mach 7.3 in the waveguide probe experiment due to a basic shortcoming in the technique itself. Therefore, the anomalous results in the lower Mach region of the microwave-horn experiment remain unexplained.

References

[1] Peperone, S. J., "X-Band Measurement of Shock-Tube Plasma Temperature," *Journal of Applied Physics*, Vol. 33, No. 2, Feb. 1962, p. 767.

[2] Gerardo, J. B., Goldstein, L., and Hendricks, C. D., Jr., "Application of Microwaves in Shock Wave Investigations," *Proceedings of the Sixth International Conference on Phenomena of Ionized Gases*, Vol. 4, 1963, pp. 331–338.

[3] Aro, T. O. and Walsh, D., "Attempted Microwave Measurement of Temperature of a Shock-Heated Plasma," *The Physics of Fluids*, Vol. 10, No. 7, July 1967, pp. 1468–1476.

[4] Aro, T. O. and Walsh, D., "Measurement of Plasma Temperature Using a Waveguide Probe," *The Physics of Fluids*, Vol. 11, No. 5, May 1968, pp. 1070–1075.

[5] Singer, A. and Minkowski, J. M., "Determination of Electron Temperature of Shock-Heated Plasma from Microwave Measurements," *The Physics of Fluids*, Vol. 16, No. 7, July 1973, pp. 1176–1177.

[6] Singer, A. and Minkowski, J. M., "Suitability of the Waveguide Probe Technique for Measuring Electron Plasma Temperature," *The Physics of Fluids*, Vol. 16, No. 11, Nov. 1973, pp. 2038–2039.

[7] Bekefi, G. and Brown, S. C., "Emission of Radio-Frequency Waves from Plasmas," *American Journal of Physics*, Vol. 29, No. 7, July 1961, pp. 404–428.

[8] Wharton, C. B., "Microwave Techniques," *Plasma Diagnostic Techniques*, edited by R. H. Huddlestone and S. L. Leonard, Academic Press, New York, 1965, pp. 477–499.

[9] Tanenbaum, B. S., *Plasma Physics*, McGraw-Hill, New York, 1967, p. 252.

[10] Heald, M. A. and Wharton, C. B., *Plasma Diagnostics with Microwaves*, Wiley, New York, 1965, p. 165.

Wall Shear and Boundary-Layer Measurements in Shock Separated Flow

PAUL J. WALTRUP* AND JAMES M. CAMERON†

The Johns Hopkins University, Silver Spring, Md.

IN Ref. 1, the instream flow structure of a nonreacting supersonic flow in a cylindrical duct containing a stabilized shock system was described and an empirical correlation for the resulting wall static pressure distribution [$p_w(s)$] and distance over which the shock pressure rise spreads (s_t) presented. These relationships, in turn, were used to predict the precombustion shock wall pressure distribution in a scramjet engine[2] since the two flows are analogous. Although these reports presented a reasonably accurate description of the over-all instream wave structure, they left to conjecture its interaction with the wall boundary-layer. This Note presents wall shear and boundary-layer pitot pressure measurements that permit a more precise definition of the flow at and near the wall in the interaction region and serve as a check on the theoretically derived turbulent boundary-layer properties used in the empirical correlation. These, in turn, allow a complete depiction of the instream and wall flow structure in a shock separated flow of this type.

Experiments

Figure 1 presents a schematic of the test apparatus, instrumentation, and flow structure generated. In each test, ambient temperature ($T_{t_0} \cong 520°R$) air is passed through a Mach 2.65 (M_a) nozzle into a 2.74-in.-diam cylindrical duct, 16.69 in. long, and discharged to the atmosphere. By lowering the tunnel total pressure (p_{t_0}), overexpanded flows are generated which create shock structures within the cylindrical test section of sufficient strength to raise the initial pressure (p_a) to the exhaust (or back) pressure (p_f). This is denoted as the shock/boundary-layer interaction region in Fig. 1 and extends over the distance s_t. Measurements of wall shear (τ_w) and boundary-layer pitot pressure (p_t') were taken in and upstream of this region at the axial stations indicated in Fig. 1 along with wall static pressures at approximately one inch intervals. Boundary-layer pitot pressure profiles were measured using two pitot rakes positioned 90° apart circumferentially for redundancy and all pressures were

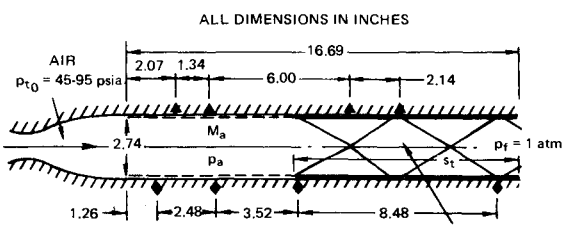

Fig. 1 Schematic of test set-up, instrumentation, and flow structure.

Received January 11, 1974. This work was supported by the United States Navy under Naval Ordnance Systems Command Contract N00017-72-C-4401.

Index categories: Nozzle and Channel Flow; Shock Waves and Detonations; Boundary Layers and Convective Heat Transfer—Turbulent.

* Section Supervisor, Supersonic Combustion, Applied Physics Lab. Member AIAA.

† Engineering Staff Associate, Propulsion Research Laboratory, Applied Physics Lab.